Autoignition-induced flashback in hydrogen-enriched laminar premixed burners

Hugo Pers, Andrea Aniello, F. Morisseau, Thierry Schuller

Autoignition-induced flashback in hydrogen-enriched laminar premixed burners

H. Pers[a,b], A. Aniello[a], F. Morisseau[b], T. Schuller[a]

[a] *Institut de Mécanique des Fluides de Toulouse, IMFT, Université de Toulouse, CNRS, France*
[b] *Hydrogen Research and Development Laboratory, SERMETA, France*

Abstract

This paper investigates the possibility of autoignition as a flashback initiation mechanism in laminar premixed burners powered by an increasing content of hydrogen in the fuel blend. A specific experimental setup provides an optical access inside a generic burner reproducing the main features of domestic boilers. This window is used to gather high-speed intensified images during transition to flashback. Zooms into the location of flashback initiation provide clear evidence for the existence of two distinct regimes. In the first one, flashback is initiated by a flame stabilized above the burner that is able to propagate upstream through one of the burner holes. In the second regime, flashback is initiated by autoignition of the fresh gases inside the burner, as they flow along the hot metallic internal wall. These observations are corroborated over a large range of equivalence ratio and hydrogen content. They demonstrate the dependence of the initiation regime on the burner wall temperature and highlight the role of the crossover temperature of hydrogen-enriched mixtures in triggering autoignition. An autoignition Damkohler number Da_i that compares a residence time of gases along the hot wall and the autoignition delay time is defined. The ratio Da_i is found to be more than an order of magnitude higher for autoignition-induced cases compared to the cases initiated by a flame propagating upstream, further supporting the existence of two distinct mechanisms leading to flashback.

Preprint submitted to International Journal of Hydrogen Energy

These results carry substantial implications on the design process of H_2-enriched laminar premixed burners.

Keywords: HYDROGEN SUBSTITUTION, PREMIXED COMBUSTION, AUTOIGNITION, FLASHBACK, FLAME-WALL INTERACTION, DOMESTIC BOILERS.

2022 MSC: 00-01, 99-00

---

1. Introduction

Reducing greenhouse gas emissions from heat production devices is a major issue for mitigating climate change. The number of investigations aimed at substituting natural gas combustion is skyrocketing. Because of the absence of CO_2 in the combustion products, and its ability to be stored and used when needed, H_2 has known a growing appeal over the last decade [1, 2]. Power-to-Gas methods aim at converting surplus of decarbonized electricity into hydrogen through electrolysis of water [3, 4], thus providing a long-term storage capacity. Hydrogen can later be either converted back to electricity through fuel cells or burnt directly. However, its strong reactivity makes the conversion of conventional burners to hydrogen challenging (see for example [5, 6, 7, 8]), highlighting the need for innovative solutions [9, 10].

The particularly high laminar burning velocity S_L of hydrogen-air mixtures proved to be an obstacle in switching natural gas burners to H_2 in industry [11, 12, 13, 14]. Most burners are designed to operate at a given adiabatic flame temperature T_{ad} that is adapted to a desired thermal load and is limited by the heat exchanger performance. For premixed domestic boilers, a reference is often set for a natural gas flame with an equivalence ratio of $\phi = 0.75$ corresponding to $T_{ad} \sim 1900$ K. If this value is to be kept constant when switching to a full-hydrogen combustion, the laminar burning velocity S_L would be 4 times larger in comparison to natural gas operation. Additionally, the quenching distance of hydrogen-enriched flames, which

drives their ability to propagate through narrow slots and to stabilize close to a flame-holder, drastically reduces with increasing hydrogen content [15, 16]. This distance was found to be directly linked to the flame thickness [17, 18]. For technologies powered by laminar flames stabilized on a perforated burner, hydrogen substitution results in higher wall temperatures, and therefore higher reactant gas temperatures [5, 19]. This higher reactivity leads to a higher propensity to flashback inside the burner [14, 20, 21] which raises important safety issues. As a consequence, the maximum hydrogen hybridization rate of existing end-use equipment designed to be operated with natural gas, propane or butane is limited to about 20% in volume [7, 22], corresponding to 7% in terms of power and CO_2 reduction.

A major research effort is being carried out to better understand the mechanisms leading to flashback. The pioneering work from Lewis [23, 24] led to the development of the critical velocity gradient theory to identify flashback limits of laminar premixed flames. It has been progressively refined for different fuel mixtures [25, 26], including effects of various parameters such as the impact of preheat temperature [27, 28]. However, this theory does not take into account additional phenomena that alter flame stabilization, such as flame stretch [29, 30], preferential diffusion [31, 32] and coupled heat exchange with the walls [33, 34, 35, 36]. Preferential diffusion is especially relevant in the case of low Lewis number fuels such as H_2 [37, 38, 39], as recently shown by numerical flow simulations attempting to extend the critical velocity gradient theory for hydrogen flames stabilized on perforated plates [40]. One of the main outcomes is the importance of the Markstein length of these flames, found to be negative for lean hydrogen-air mixtures [41]. Its impact on flame stabilization had to be taken into account to correctly predict flashback limits of flames stabilized on a flame-holder [42, 43, 40].

Although numerous studies investigated flame stabilization on perforated plates

[42, 44] and on burners used in domestic boilers [45, 46], detailed experimental investigations on flashback in laminar multi-perforated burners remain scarce, especially at high H_2-hybridization rates. As the hydrogen content increases, the burner temperature can exceed 1000 K. The hole size of these burners is of the same order of magnitude as the hydrogen flame quenching distance [47]. Reducing the hole diameter prevents, in most cases, the flame from instantly propagating upstream through the injection holes at ignition.

In a recent study on the impact of hydrogen addition on flashback limits, the importance of the thermal state of the burner has also been stressed out [5]. Two different flashback categories were identified: (i) instantaneous flashback, that happens immediately after ignition of a cold burner at a given flow rate, equivalence ratio and hydrogen hybridization, and (ii) flashback taking place after a thermal transient state, during which the wall temperature slowly increases until reaching a specific threshold value defined as $T_{w,f}$. It was shown that this threshold temperature could exceed 1100 K depending on the equivalence ratio and the hydrogen hybridization rate PH_2, expressed in terms of power originating from hydrogen combustion for a given thermal power output. It was also found that the critical velocity gradient theory fails to reproduce the flashback limits in these conditions.

These transient phenomena associated with high wall temperatures lead to consider the possibility of autoignition of the combustible mixture alongside the inner burner walls. Indeed, hydrogen has long been identified as a highly reactive fuel, more prone to autoignition than hydrocarbon fuels [48, 49]. Several studies have highlighted the existence of a crossover temperature for hydrogen-air mixtures, above which a chain-branching explosion path leads to a sudden decrease in the autoignition delay time [50, 51, 52], that eventually causes the reactants to autoignite. However, investigating

the flashback dynamics in multi-perforated domestic burners is challenging: first, because its initiation point is not known in advance, and second because of the difficulty to get an optical access to the internal side of the burner metallic walls.
The objective of this study is to evaluate the impact of wall temperature on flashback for H_2-enriched methane-air flames, by investigating the possibility of autoignition as a flashback initiation mechanism with a set of experiments. This paper is organized as follows. A specific experimental setup with a large optical access to the internal side of a perforated cylindrical burner is presented in the following section, along with the diagnostics used to investigate flashback. The flashback initiation and dynamics inside the burner are then investigated, for typical cases with wall temperatures below and above the crossover temperature of the reactive mixture. Two regimes of flashback are identified and their dynamics is analyzed. Finally, conclusions shed light on the origin of flashback in multi-perforated laminar premixed burners when switching from natural gas to hydrogen.

2. Materials and methods

2.1. Experimental setup

Figure 1 shows a schematic of the experimental setup. A cylindrical burner is fixed on the top of a converging nozzle transition piece set above a 100 mm diameter cylindrical plenum. The plenum is supplied at one boundary with methane-hydrogen/air mixtures at atmospheric pressure and temperature. A bronze porous medium with a 40 μm pore size and a 4 mm thickness is placed at the other plenum boundary, acting as a flame arrestor and adding a pressure loss of about 500 Pa for typical low power operating conditions of the burner. The whole setup is positioned horizontally to facilitate the optical access through the burner. The cylindrical

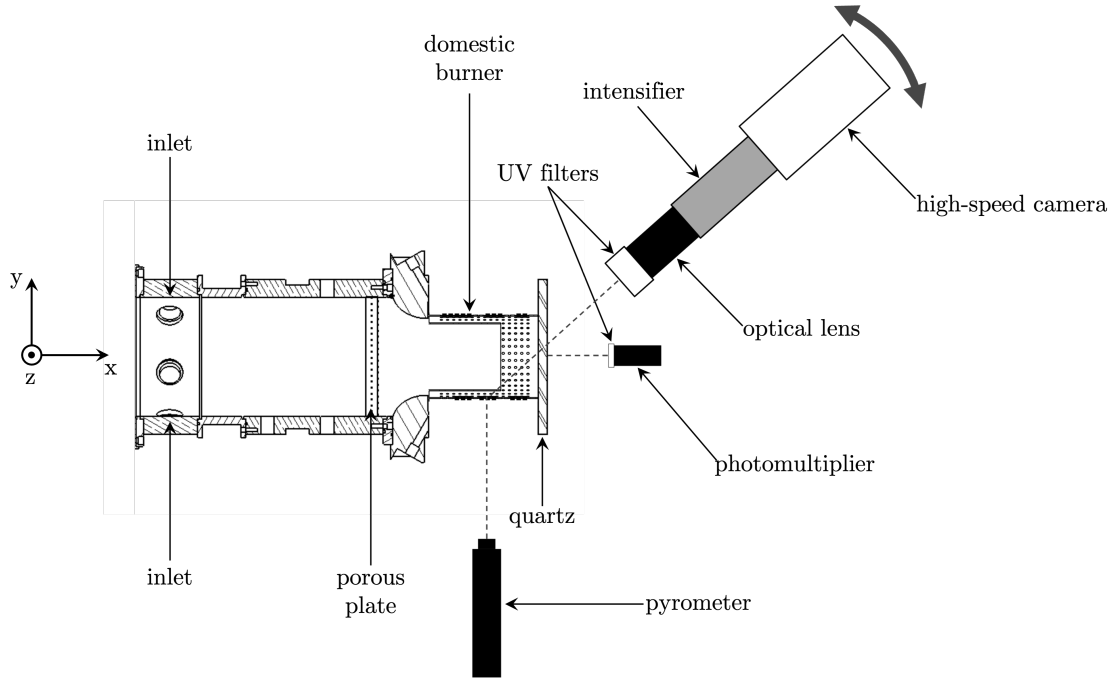

Figure 1: Top view of the experimental setup. The curved double arrow illustrates the displacement of the imaging setup when switching from an internal side view to a front view. The z-axis corresponds to the normal to the floor plane.

burner has been modified by removing its metallic top which has been replaced by a transparent 8 mm thick disk made of fused silicate. This window is maintained compressed against the metallic burner using spring loaded screws that are fixed to the plenum. These fixations are not reproduced in Figure 1. Springs allow to maintain the contact between the window and the metal and accommodate with the different thermal expansions of the materials. Leaks are prevented by a layer of fiberglass placed at the cylindrical burner periphery between the burner and the quartz window.

The flow rates are regulated individually using Bronkhorst F-201CV mass flow

controllers. A pressure relief valve, set to open if the over-pressure reaches 1 bar, is installed in the plenum.

2.2. Burner description

A side view of the burner is pictured in Figure 2. This generic burner with an optical access shares the main features of standard burners used in domestic boilers. It is designed to operate between 3 and 30 kW, which is a common range for boilers destined to domestic use. The height and diameter of the studied burner are respectively 91 mm and 70 mm. It is formed by a 0.6 mm sheet made of refractory steel that is bent and welded to form a cylinder. The cylinder is perforated with a specific geometrical pattern. Each pattern unit is made of two holes and two slots and defines a patch that is reproduced periodically over the burner length and circumference. The power range can be modified by using a shorter or a longer burner, and by adapting the heat exchanger accordingly. The low power configurations are commonly used in residential boilers. The largest ones produce a thermal power up to a few MW and can supply industrial heat exchangers. They were initially designed to optimize the operating range with natural gas or propane by improving their resistance to blow-off. The burner used in this study features 11 rows of 57 patches. The only asymmetry of the burner geometry is the weld sealing the cylinder that is shown in Figure 2. This welded surface covers a relatively substantial surface area without perforations similar to a missing column of holes. For this specific burner, the diameter of the holes is 0.7 mm and the slots are 0.1 mm large and 3.5 mm long.

During normal operation with natural gas, the combustion reaction spreads uniformly over all the perforations of the burner surface, except for a minor difference at the top due to natural convection. Because of the complex geometry of the burner

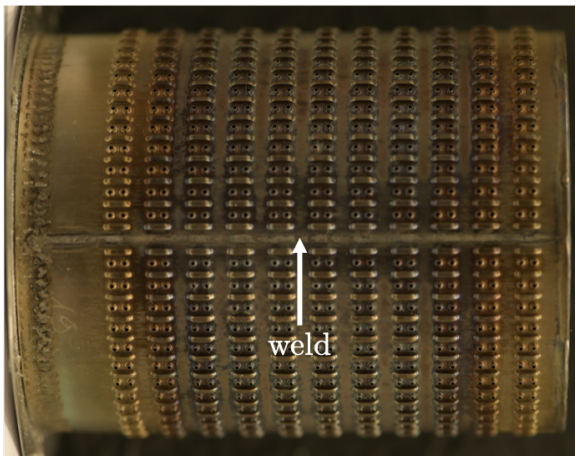

Figure 2: Side view of the cylindrical burner. The weld is visible at the center.

perforations and of the heterogeneous flow field inside the burner cavity, a mean value for the bulk flow velocity U_b inside a single hole is used as a reference to compare the different cases explored. This reference velocity U_b is deduced from the total mass flow rate through the burner:

$$U_b = \frac{\dot{m}_h}{\rho_u A_h} = \frac{\sigma \dot{m}_p}{\rho_u A_h N_p} \tag{1}$$

where $\dot{m}_h$, $\dot{m}_p$, ρ_u, N_p, σ and A_h are respectively the mass flow rate through a single hole, the mass flow rate through a patch (i.e. two holes and two slits) [5], the density of the preheated gases at T_u, the total number of patches, the ratio of a hole surface over a patch surface, and the surface area at the outlet of a single hole.

2.3. Optical diagnostics

A Nikon D8500 camera with a 105 mm lens provides color images of the burner. High-speed intensified imaging is used to monitor flashback initiation. It is conducted with a Phantom V1612 camera equipped with a Lambert HiCATT intensifier and a Micro-Nikkor 105 mm UV lens, allowing to record the UV signal emitted by studied

flames. Indeed, the important share of hydrogen in mixtures makes the visible signal weak and difficult to interpret, emission being mainly condensed around 310 nm due to OH^* radicals and the absence of CH^* radicals [53]. A 305-315 nm band pass filter is used to center the observation on OH^* emission. Because of the very quick production and consumption of OH^* radicals in the flame, its monitoring allows to sharply locate the reaction front of laminar premixed flames [52].

Two camera positions are investigated to modify the field of view. First, the camera is placed along the axis of the burner at the location of the photomultiplier as in Figure 1. Second, it is placed at a 35° angle relative to the burner axis, to focus on the flashback initiation region, as illustrated in Figure 1. The camera and the setup remain in the same vertical plane parallel to the ground.

A Hamamatsu H10722-04 photomultiplier (PM), with a spectral response between 185 nm and 870 nm and a maximum frequency of 20 kHz, is also used to record the global light intensity emission during flashback. The PM is placed in front of the quartz window and records a signal integrated along the line of sight. A 305-315 nm band pass filter is also added to reduce the noise and focus on the OH^* radical emission. As its position is not compatible with the camera being located in front of the burner, the PM is only used with the camera at a 35° angle relative to the burner axis (see Figure 1).

2.4. Burner and gas temperature measurements

The wall temperature T_w of the external wall of the burner is measured using a bichromatic infrared pyrometer (FLUKE Endurance Series) with a 1.6 μm nominal spectral response that is sensitive to temperatures between 250°C and 1200°C. The temperature is retrieved considering the signal emitted by a 4 mm diameter target spot on the metallic surface.

Because of the heat exchange between the fresh gas and the hot metallic walls, the temperature of the combustible mixture T_u flowing through the burner holes is higher than the inlet gas temperature $T_{in} = 300$ K injected in the plenum. This temperature is here deduced by using the technique presented in [5, 54]. The burner is first ignited at the targeted stable operating condition. Once the thermal steady state is reached, the fuel is shut down while the air flow rate is kept constant. Then, a K-type thermocouple with a 1.5 mm spherical junction is placed downstream of a hole in the hot stream of gases. The measurement of the gas temperature is initially affected by the thermal inertia of the thermocouple, which leads to consider only the exponential temperature decay recorded after this transient phase. In this regard, the influence of the wall thermal radiation on the gas temperature measurement is demonstrated to be negligible in Appendix A and is therefore disregarded. As illustrated in Fig. 3, an extrapolation based on the gathered data allows to estimate the fresh gas temperature T_u at the initial instant. Examples of results are presented in Figure 3, where the indicated value T_u is the mean of at least three independent measurements. The confidence interval is roughly $\pm 3\%$, showing a great repeatability of the results.

2.5. Experimental methodology

The analysis focuses on flashback taking place when the burner metallic envelope temperature T_w becomes high enough, above 500 K. In these cases, flames are stabilized after ignition above cold surfaces and the burner temperature increases over time until reaching a certain threshold temperature $T_{w,f}$, above which flashback takes place as described in [5]. Flashbacks taking place right after ignition of the cold burner are not considered in this study.

Experiments are made as follows: the mass flow rates of fuel and air are set in order to reach the desired equivalence ratio, H_2-hybridization rate and thermal power.

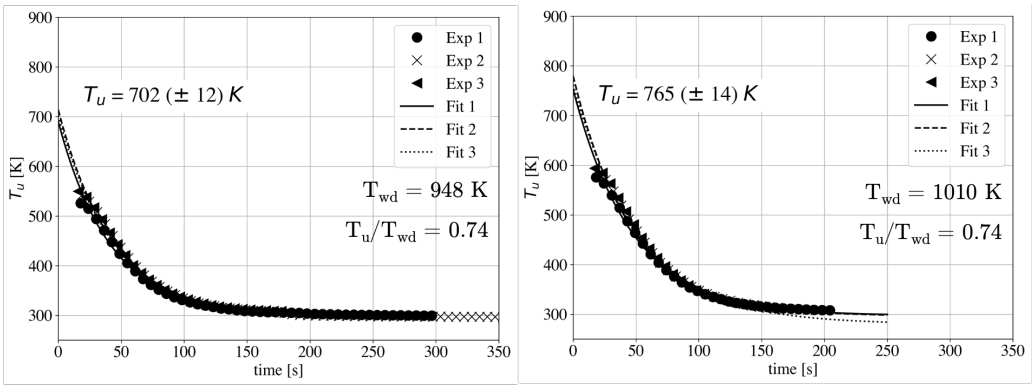

(a) $\phi = 0.65$, $PH_2 = 60\%$ (b) $\phi = 0.80$, $PH_2 = 50\%$

Figure 3: Examples of determination of the preheated temperature T_u from the combustible mixture leaving the burner holes deduced from exponential extrapolation of experimental data. Two operating conditions are presented. The external metallic surface temperature T_w is 948 K (top) and 1010 K (bottom), leading to $T_u/T_w \simeq 0.74$ in both cases.

The burner is then ignited. If the burner wall temperature T_w reaches an asymptotic steady state value and does not flashback after 5 minutes, the operating condition is considered to be stable. If flashback occurs during the transient temperature increase of the burner wall, these conditions are further investigated. After flashback, fuel supply is shut and the burner is only fed with air until it cools down. The window made of quartz having the highest thermal inertia compared to the other thin metallic components, the burner is re-ignited once the external surface of the window reaches ambient temperature.

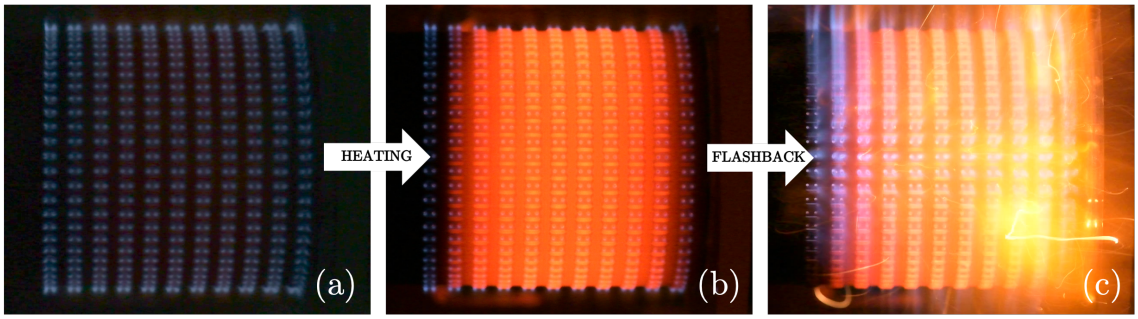

Figure 4: Flashback sequence recorded by a color-camera at 60 frames per second. Conditions are $\phi = 0.78$, $P_{H2} = 65\%$, $P = 3$ kW.

3. Results and discussion

3.1. Flashback limits and impact of the burner thermal state

The regime of interest corresponds to flashback occurring during the transient thermal state of the burner after ignition for a fixed flow rate, equivalence ratio and hydrogen enrichment. Figure 4 illustrates the three steps of a typical flashback event observed in this regime, as captured by a Nikon D8500 camera at 60 frames per second. Image (a) is right after ignition. The flames are all well stabilized over each perforation. The burner wall temperature clearly increases between images (a) and (b). Both ends of the burner remain colder due to heat losses to the plenum (on the left) and to the window (on the right). Flashback takes place between images (b) and (c). Image (c) shows the outer flames being blown off accompanied by a violent sound pressure peak. Blow off is the consequence of the rapid gas expansion caused by the flame suddenly propagating inside the burner.

Figure 5 shows a contour map of adiabatic flame temperatures T_{ad}, as a function of equivalence ratio and H_2-hybridization power rate PH_2. Adiabatic flame temperatures T_{ad} of methane/hydrogen/air mixtures are calculated at $p_a = 1$ *bar* with the 1D-flame solver CANTERA using the GRI-MECH 3.0 mechanism for gases

injected at $T_a = 300$ K. The red dashed line illustrates the reference temperature $T_{ad} = 1915$ K, corresponding to a methane/air flame at $\phi = 0.75$. The equivalence ratio must be reduced to about $\phi = 0.64$ for a hydrogen/air mixture to keep the same adiabatic temperature. The solid line with triangle markers exhibits the flashback limit of the burner for 3 kW thermal power. The flashback boundary was obtained by firing the burner with increasing contents of hydrogen at a given equivalence ratio, until flashback occurs. This process was repeated for a wide range of equivalence ratio. The target burnt gas temperature $T_{ad} = 1915$ K becomes unreachable for combustible mixtures with hydrogen concentrations $PH_2 > 60\%$ because of flashback. In the following, flashback is investigated at operating conditions close to the iso-line of interest $T_{ad} = 1915$ K.

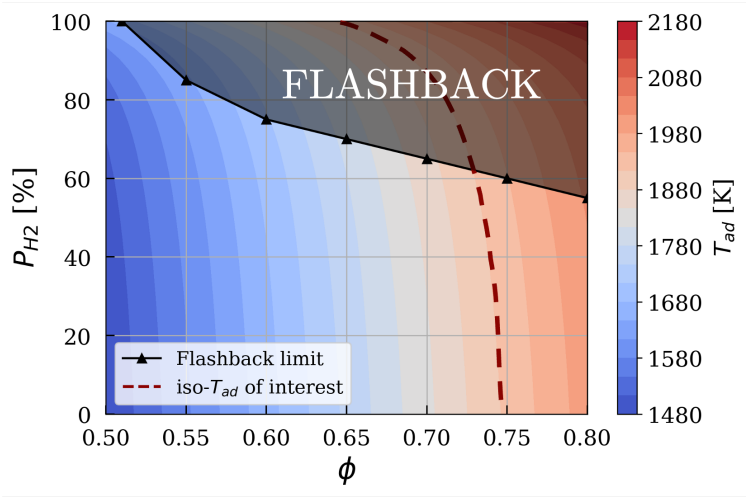

Figure 5: Adiabatic flame temperature map and flashback limits of the burner at 3 kW, $p_a = 1$ bar.

A key parameter for flashback is the preheat temperature T_u of the reactants leaving the burner holes. In a previous study made on a similar setup [5], a proportional relation was found between the wall temperature T_w and preheat temperature T_u when the burner was operated at thermal powers around 3 kW. To find an analogous

relation in the present case, the preheat temperature T_u is determined for different operating conditions using the method described in Section 2, for burner wall temperatures T_w ranging between 950 K and 1100 K (Figure 3). For the studied burner, the ratio of preheat temperature over wall temperature T_u/T_w turns out to be quasi-constant from an operating point to another, leading to the following empirical expression valid at $P \approx 3$ kW and for T_w between 950 K and 1100 K:

$$T_u \simeq 0.74 T_w \tag{2}$$

This relation is used in the following to estimate T_u from measurements of T_w and determine the corresponding bulk flow velocity U_b of the reactants flowing through a single hole. The same value is also used to determine the laminar burning velocity S_L of the combustible mixture with an inlet temperature T_u. The ratio $(U_b/S_L)_{T_u}$ describes the kinematic balance between the fresh gases velocity and the flame front propagating in the normal direction towards the reactants. Keeping this ratio constant suppresses the influence that would have a hydrodynamic imbalance between two cases. An increase in burner temperature T_w was found to trigger flashback for a burner hybridized with increasing H_2 concentrations in [5], drastically limiting the operating range for hydrogen-enriched combustible mixtures. High-speed imaging is now used to identify the origin of flashback when the hydrogen content is increased.

3.2. Preferential flashback initiation zone

At first, flashback is investigated using the high-speed camera placed along the burner axis in front of the quartz window. This front view is used to infer the location of flashback initiation, observe flame front propagation, and measure the speed at which the flame front propagates inside the burner during flashback. Figure 6 displays

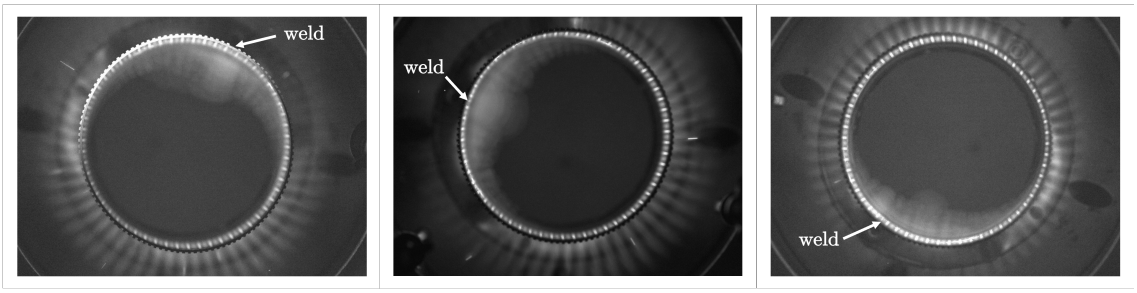

(a) rotation 1 (b) rotation 2 (c) rotation 3

Figure 6: Selected images of flashback initiation for different weld positions with respect to the vertical direction. Conditions are $\phi = 0.67$, $PH_2 = 80\%$ and $P = 3$ kW.

images at the first instants of flashback taken with the high speed camera for different burner rotations, the weld being located at the top in (a), on the upper left side in (b) and at the bottom in (c). Conditions are $\phi = 0.67$, $PH_2 = 80\%$ and $P = 3$ kW. These images are recorded without light intensifier in front of the high speed camera. Flashback initiation appears to be located close to the weld in these three cases and this observation is corroborated for most of the studied cases over more than 50 tests.

To further examine the role of the weld on flashback initiation, the distribution of the wall temperature T_w around the burner is investigated at the mid height of the burner. Figure 7 shows the wall temperature measured along the circumference of the burner, as a function of the angle θ with respect to the weld position. Temperature profiles are presented for two operating conditions corresponding to stable cases with a temperature gap around 100 K to ensure the validity of the observations made over a relatively large range of burner temperatures T_w. Hot gas buoyancy explains the important temperature difference between the top of the burner at $\theta = 90°$ and the bottom at $\theta = -90°$, a smaller flow rate leading to flames stabilized closer to the

wall at the bottom. The wall temperature T_w drops at the exact position of the weld, at $\theta = 0°$, where there is no flame. This is consistent with the absence of flame directly above the weld, limiting the heat load in this region of the burner. However, the wall temperature abruptly peaks at hole patches right next to the weld position. These peaks result from a longer preheat of reactants flowing against the hot wall in the vicinity of the weld, that causes flames to stabilize closer to the wall and therefore enhance wall temperature. As it increases yet again the reactants preheat temperature, this feedback mechanism tends to further increase the wall temperature and aggravates the flashback propensity. This already gives some insight on the observations made in Figure 6 with flashback initiations taking place close to the weld. The fact that this phenomenon is observed for numerous weld positions demonstrates its governance over flashback initiation.

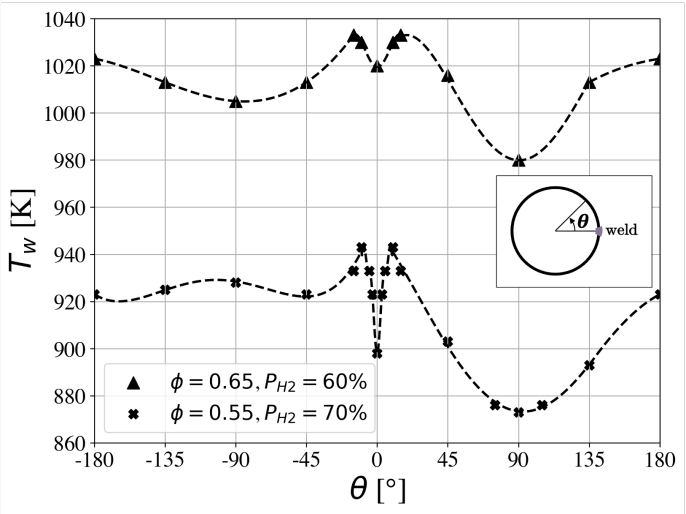

Figure 7: Burner temperature T_w as a function of the azimuthal angle θ, increasing clockwise, $\theta = 0°$ being the weld position (fixed on the right side).

It is important to mention that, for a given operating condition, the wall temperature $T_{w,f}$ at which flashback occurs is highly repeatable, as illustrated in Figure 8. The

three tests lead to a flashback at an almost constant temperature $T_{w,f}$, within ± 5 K, and at a very similar delays after ignition, within ± 5 s. This temperature threshold $T_{w,f}$ exists for every points investigated in this study. However, the value for $T_{w,f}$ varies to a great extent for different mixtures, equivalence ratios and H_2-hybridization rates. For all conditions explored, flashback takes place for wall temperatures ranging from 900 K up to 1100 K.

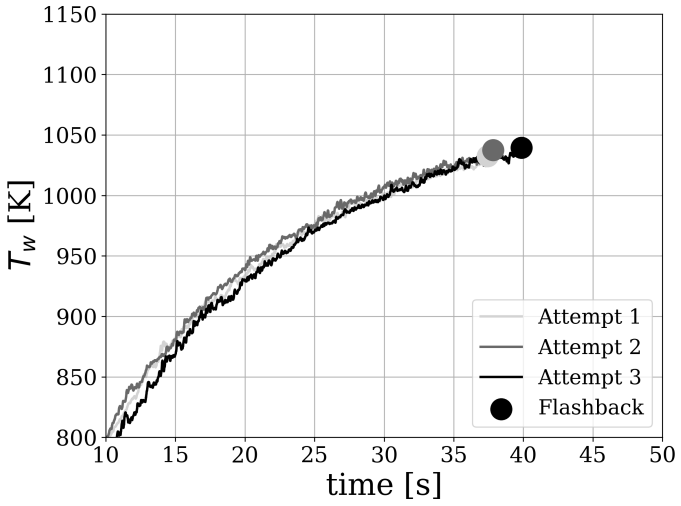

Figure 8: Example of flashback repeatability for a given operating point, $\phi = 0.76$, $PH_2 = 60\%$, $P = 6$ kW.

3.3. Flame front propagation during flashback

Transition to flashback of two H_2-enriched combustible mixtures, defined as case A and case B, are now investigated using high-speed intensified imaging. Cases A and B differ by their equivalence ratio and hydrogen hybridization rate which are respectively $\phi^A = 0.6$, $PH_2^A = 100\%$, $P^A = 3$ kW and $\phi^B = 0.75$, $PH_2^B = 67\%$, $P^B = 3.25$ kW. The wall temperature leading to flashback also differs $T_{w,f}^A = 953$ K and $T_{w,f}^B = 1053$ K. These flames were selected because the flashback temperature

$T_{w,f}$ differs by about 100 K, while the ratio of bulk velocity over laminar burning velocity at the preheat temperature T_u measured in the experiments, $(U_b/S_L)_{T_u}$, remains almost the same in both cases, being respectively 0.64 and 0.62. Propagation of the flame front during flashback for cases A and B is presented in Figure 9. Associated videos are provided as supplementary material. The weld position is indicated by a white cross, and the position of the burner wall is delimited by a white dashed circle. A colormap for the light intensity is added to facilitate flame front tracking.

At first glance, on Figure 9, flashback dynamics appears to be very similar in both cases. Flashback initiation takes place in the neighborhood of the weld at the right in the figures in the two cases. As the flame propagates inside the burner, gas expansion through the flame front pushes the reactants towards the side opposed to the initiation point, where flames appear elongated before being blown off. In the vicinity of the weld, flame expansion leads to a relatively hemispherical flame propagation at the first instants after flashback. The metal in this region was shown to reach higher wall temperatures, most likely due to a higher preheat of the reactant gases next to the weld. The hotter reactant gases are consistent with a faster expansion of the flame front in this region, which may explain the large hemispherical front observed at the weld in both cases.

Another consideration in Figure 9 is the striking difference between flame front propagation towards the center of the burner and along the metallic wall of the burner. The absolute propagation velocity of these reaction fronts can be estimated as follows. The burner radius being R_b, the flame propagation velocity at the wall $S_{d,w}$ is deduced from the time needed by the flame leading edge to cover half a perimeter πR_b along the burner wall between the initiation point and a diametrically opposite point. The velocity at the center $S_{d,c}$ is estimated as the time needed

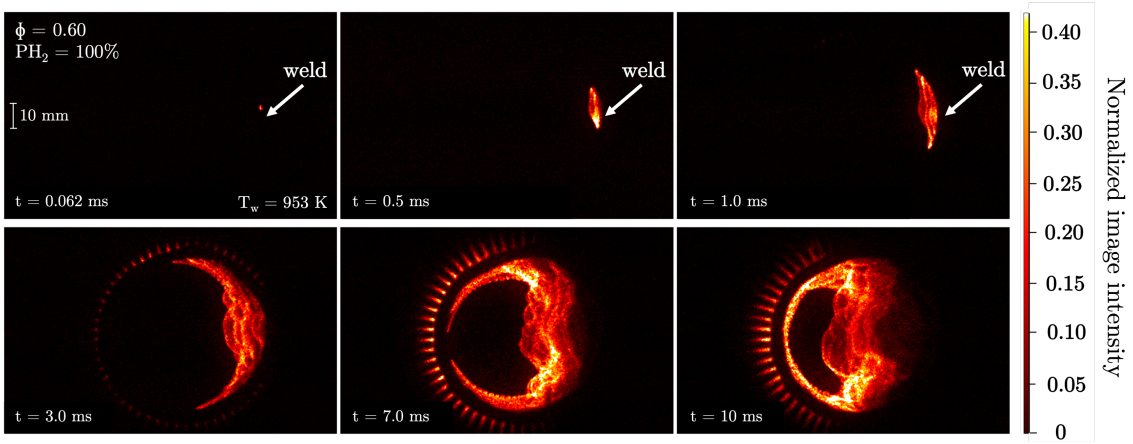

(a) case A: $\phi = 0.6$, $PH_2 = 100\%$, $P = 3$ kW

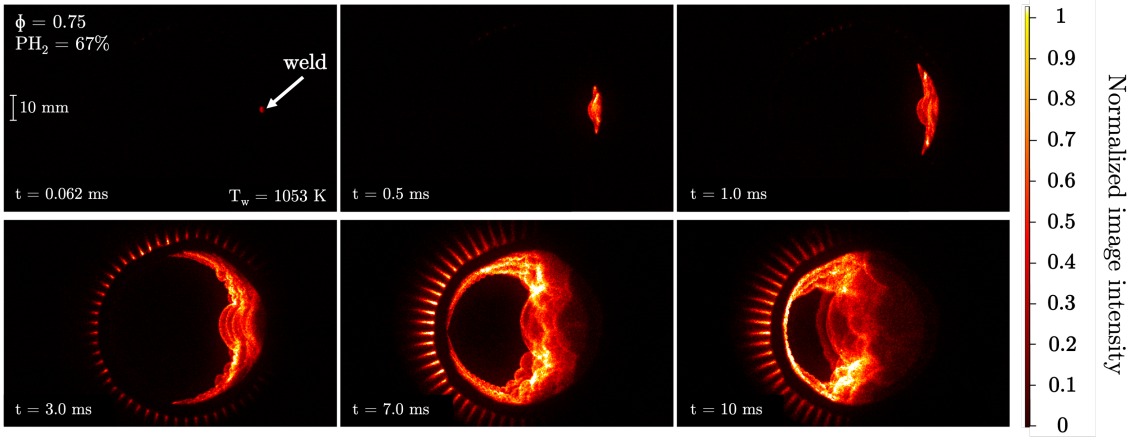

(b) case B: $\phi = 0.75$, $PH_2 = 67\%$, $P = 3.25$ kW

Figure 9: Comparison of the flame front propagation during flashback for (a) a relatively low wall temperature $T_{w,f} = 953$ K and (b) a relatively high temperature $T_{w,f} = 1053$ K. Weld position is indicated by the white cross.

by the flame front to cross a burner diameter $2R_b$ from the initiation location and passing through the burner axis. These velocities deduced from sequences of images

Table 1: Comparison, for cases A and B, of equivalence ratio ϕ, H_2-hybridization power rate PH_2, wall temperature at flashback $T_{w,f}$, front absolute displacement speed along the wall $S_{d,w}$ and through the center of the burner $S_{d,c}$, estimated reactant mixture temperature T_u^* deduced from a 1D laminar burning velocity corresponding to $S_{d,c}$, and T_u obtained from empirical correlation Eq. (2).

	ϕ	PH_2	$T_{w,f}$ (K)	$S_{d,w}$ (m/s)	$S_{d,c}$ (m/s)	$T_u^*(S_{d,c})$ (K)	T_u from Eq. (2) (K)
Case A	0.60	100	953	15.0	5.4	657	705
Case B	0.75	67	1058	16.5	5.7	736	783

as shown in Figure 9 are reported in Table 1. In both studied cases, it appears that the flame propagates 3 times faster along the wall than through the center of the burner. This comes out as a direct consequence of the high temperature of the wall that preheats reactant gases circulating nearby compared to cooler reactants in the center of the burner away from the solid walls. These measurements clearly show that this substantial preheating results in an acceleration of the flame front propagation along the burner wall.

As the flame is also advected by the local flow, another mechanism that could result into a faster propagation of the flame along the burner wall is a smaller local flow velocity because of the no-slip condition at the wall. To evaluate this effect, additional experiments were carried out with flashback taking place instantaneously after burner ignition. In this flashback regime studied in [5], the metal of the burner wall remains cold. Figure 10 shows images of flashback in a burner featuring holes with a larger diameter $d = 0.9$ mm, but with a global porosity identical to the studied burner. The burner is ignited from the left side in Figure 10. The flame front then impinges the burner external surface at $t = 0$ ms and crosses the perforated wall immediately at

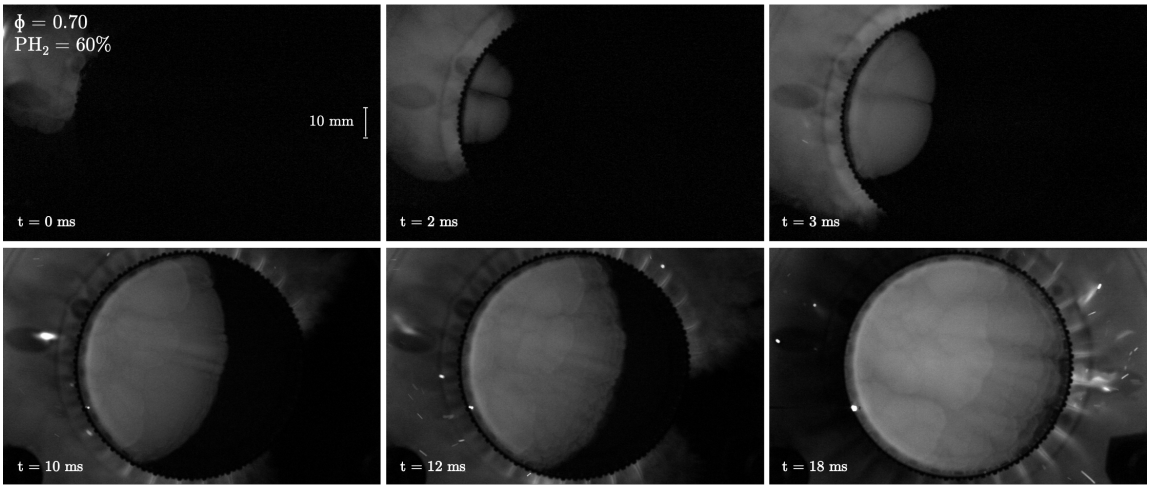

Figure 10: Example of flashback with a burner with 0.9 mm hole diameter, at $\phi = 0.70$, $PH_2 = 60\%$, $P = 3$ kW. Flashback starts immediately at ignition (top left frame), with cold walls.

$t = 2$ ms. The propagation of the flame inside the burner remains hemispherical until it fills all the burner volume at time $t = 18$ ms. During the entire duration of the flashback, there is no visible heterogeneity in the flame front propagation between the wall and the center of the burner. In this case, the fresh gases mixture has roughly the same temperature at the center and along the cold burner wall. This additional test confirms the thermal origin of the asymmetrical behavior observed in Figure 9, with a propagation of the flame that is much faster along the wall than through the center of the burner because of the preheating of the combustible mixture along the wall.

Neglecting the very small radial velocity of the reactants flowing through the burner, the measured absolute propagation velocities $S_{d,w}$ and $S_{d,c}$ of the flame arms with respect to a fixed coordinate system can be assimilated as a first approximation to flame displacement speeds relative to the fresh reactants. The difference of displacement speeds measured for cases A and B in Table 1 is small, which is

consistent with a constant ratio of bulk velocity over laminar burning velocity for gases preheated by the hot wall, $(U_b/S_L)_{T_u}$. The preheat temperature of the reactants far from the wall can be estimated using the flame displacement speed $S_{d,c}$, measured at the center of the burner. Indeed, a rough estimate is to consider the displacement of the leading edge front through the center of the burner as a one-dimensional freely adiabatic propagating flame. Given the inlet mixture composition and pressure, the laminar burning velocity S_L only depends on the inlet temperature. Therefore, 1D freely-propagating flames are simulated using the CANTERA solver at both operating conditions by varying the inlet temperature. This temperature is iterated until the calculated laminar burning velocity S_L matches the observed flame displacement speed $S_{d,c}$. The corresponding inlet temperatures, defined as T_u^*, are reported in Table 1. These temperatures can also be compared to T_u deduced from Eq. (2). The temperatures T_u^* and T_u are close, T_u^* being about 7% smaller than T_u. This gap is consistent with the fact that T_u^* is estimated for reactants far from the wall, when T_u is measured in gases leaving the burner perforated wall, which are hotter. The fact that T_u^* and T_u are in the same range, although obtained by two independent means, supports the previous estimation of the ratio of bulk velocity over laminar burning velocity (U_b/S_L) at the correct preheat temperature T_u of the reactants.

Flame front propagation during flashback has been shown to be highly sensitive to the thermal state of the burner, the heat transfer from the hot burner wall to the nearby reactants accelerating the flame propagation along the wall. The two studied cases of flashback occurring at different wall temperatures display initiation points close to the weld, which leads to consider the possibility of autoignition as a flashback initiation mechanism.

3.4. Crossover temperature and autoignition delay time

Flashback for cases A and B, featuring a large volumetric hydrogen content in the fuel blend, take place at relatively high wall temperatures: $T_w^A = 953$ K and $T_w^B = 1053$ K. These values are close to the cross-over temperature $T_c \approx 950$ K at $p_a = 1$ bar for typical H_2/air mixtures [52], which is defined as the temperature for which chain-branching steps rate equals the recombination reaction rate. Below the crossover temperature T_c, the recombination reaction $H + O_2 + M \rightarrow HO_2 + M$, M being a third body, keeps the concentration of H radicals at low levels, therefore avoiding a chain-branching explosion in favor of a slower thermal explosion [51, 52]. Above the crossover temperature T_c, a chain-branching path described by the overall reaction $3H_2 + O_2 \rightarrow 2H_2O + 2H$ progressively takes control of the autoignition kinetics, as the sudden growth of H radical concentration rapidly reduces the autoignition delay time.

As temperature T_w^A is close to the crossover temperature estimated in [52], and T_w^B is 100 K higher, it is necessary to confirm the potential difference in autoignition delay times between the two cases, that could eventually lead to different flashback mechanisms. Therefore, autoignition delay times of $CH_4 - H_2/air$ mixtures are calculated using CANTERA, with the GRI-MECH 3.0 mechanism, for varying gas temperature and hydrogen power substitution rate PH_2 at $\phi = 0.6$. The autoignition delay time τ_i is estimated as the time at which OH^* radicals concentration peaks [55]. Results are presented in Figure 11. When the gas temperature exceeds $T_u = 950$ K, which roughly corresponds to the crossover temperature determined in [52], a very fast decrease of the ignition delay time τ_i is observed. Indeed, when considering examples of case A at $T_w^A = 953$ K and case B at $T_w^B = 1053$ K, autoignition delay times differ by more than an order of magnitude, from $\tau_{AI}^A \sim 8$ ms to around $\tau_{AI}^B \sim 0.3$ ms. It can also be noticed that the autoignition delay τ_i greatly decreases as soon as

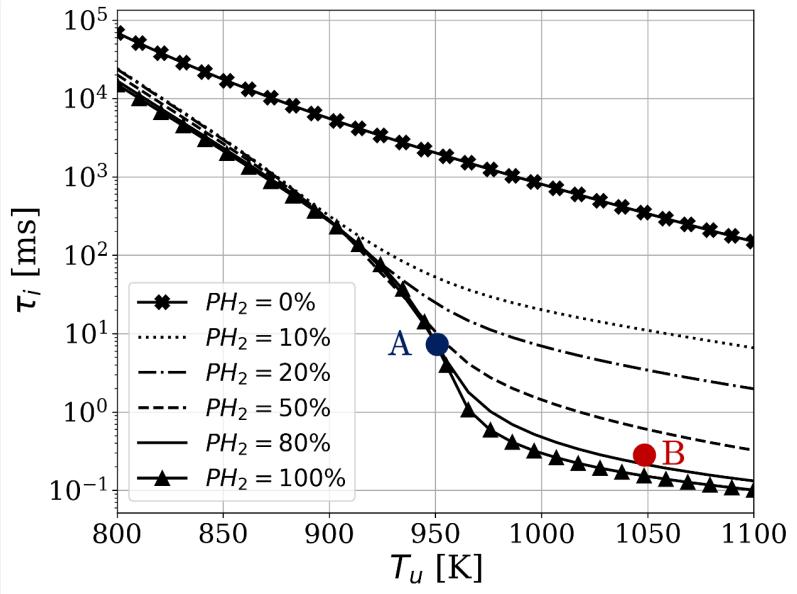

Figure 11: Evolution of ignition delay time for $CH_4 - H_2/air$ mixtures at $\phi = 0.6$, as a function of inlet gas temperature T_u and H_2-hybridization power rate PH_2. Studied cases A and B are represented by the filled circles.

hydrogen is added in the fuel, but that the sudden drop at crossover temperature T_c becomes significant for $PH_2 > 50\%$, corresponding to a volumetric H_2-hybridization of 80%. Consequently, for the highly H_2-hybridized conditions investigated in this study, where $65\% \leq PH_2 \leq 100\%$, the crossover temperature T_c can be considered as almost constant, the main difference being the absolute value of autoignition delay time τ_i reached above T_c.

The disparity of wall temperature between $T_w^A = 953$ K and $T_w^B = 1053$ K appears to cause an important variation of autoignition delay times, because of the change of hydrogen-air chemistry taking place around 950 K. Short ignition delay time could potentially lead to autoignition if the residence time of reactant flow is sufficiently large.

A closer look at Figure 9 with a zoomed view reveals a small difference of flashback initiation point, located along the weld in case B and slightly above in case A. This difference is investigated in the following section by adapting the camera view field.

3.5. Propagation vs autoignition flashback regimes

The high-speed camera is now positioned off axis with a field of view focusing on the preferential flashback initiation zone around the weld. Figure 12 displays flashback initiation sequences for case A and case B, side-by-side. Flashback videos can be found in the supplementary material. High-speed images are recorded with a frequency of 16 kHz, enabling to identify initiation locations. These points are highlighted on the second row in Figure 12 with close-up inserts. Two different locations of flashback initiation can clearly be identified. It occurs inside a hole in case A (propagation regime) and is triggered from the inner wall along the weld in case B (autoignition regime).

Experiments in each regime were repeated 10 times to exclude the possibility of a marginal phenomenon. An example of distribution of flashback initiation locations for typical conditions corresponding to each regime is presented in Figure 13. The number next to each initiation point corresponds to the number of tests resulting in flashbacks starting at this specific location. For a given operating condition, the same flashback regime is observed each time the experiment is repeated. In most cases, flashback initiation takes place around the weld. For the first case (a), the only change is the location of initiation hole. For the second case (b), the initiation point marginally moves along the weld.

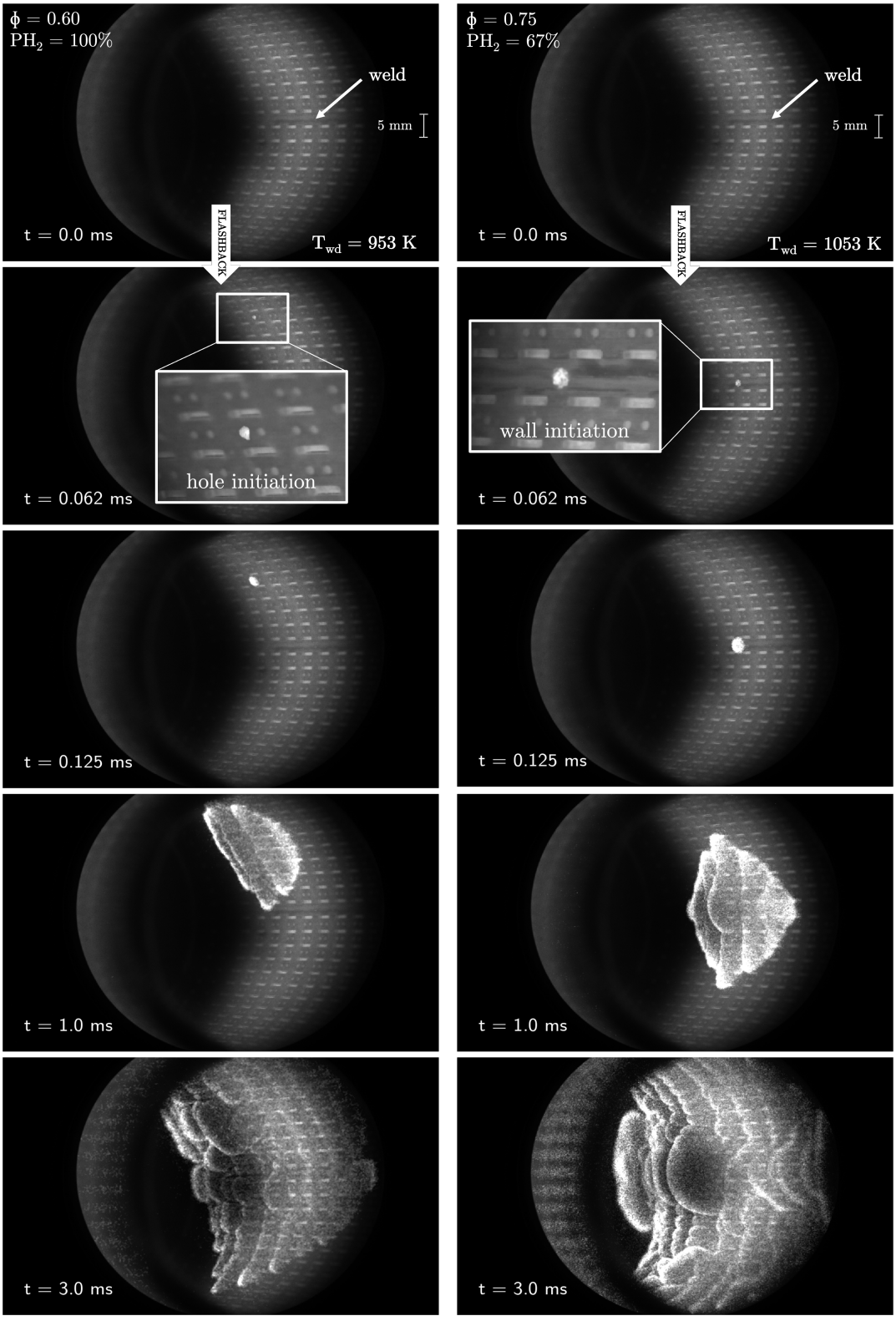

(a) case A: $\phi = 0.6$, $PH_2 = 100\%$, 3 kW (b) case B: $\phi = 0.75$, $PH_2 = 67\%$, 3.25 kW

Figure 12: Comparison of internal views of flashback initiation and propagation, for two regimes of flashback: hole initiation (a) and wall initiation (b). T_{wd} is the temperature at the weld.

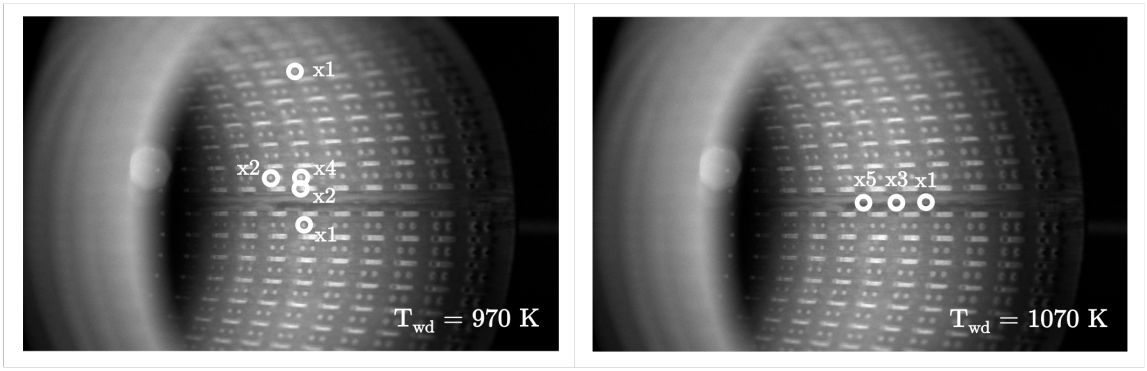

(a) Hole initiation: $\phi = 0.67$, $PH_2 = 80\%$ (b) Wall initiation: $\phi = 0.82$, $PH_2 = 60\%$

Figure 13: Flashback initiation point distribution for a set of operating conditions in regime FB-H (a) and FB-AI (b). Symbol "xN_b" next to each point corresponds to the number N_b of results with initiation at this location.

These observations corroborate the existence of two flashback regimes when the burner temperature reaches $T_c \sim 950$ K. In the first regime, designated as regime FB-H for flashback originating from a hole, the flame stabilized above the perforated plate is able to propagate upstream through a hole of the burner. This standard flashback mechanism takes place when the wall temperature remains below or close to $T_c \sim 950$ K. In the second regime, reached for higher wall temperatures and designated as regime FB-AI for flashback originating from autoignition, the combustible mixture appears to ignite itself nearby a hot wall inside the burner.

To support this observation, a set of operating conditions that allows a clear repeatable identification of the flashback initiation location is investigated. At first, points are chosen so that the ratio of bulk velocity over laminar flame burning velocity at preheat temperature T_u remains quasi-constant at $(U_b/S_L)_{T_u} \approx 0.6$. The ratio $(U_b/S_L)_{T_u}$ can hardly be estimated ahead of the experiments, as the wall temperature

$T_{w,f}$ at flashback and therefore T_u highly depend on the selected operating point. Conditions fulfilling $(U_b/S_L)_{T_u} \approx 0.6$ are therefore identified afterwards. The list of studied operating conditions, wall temperatures T_w and preheated gas temperatures T_u, as well as the nature of the flashback observed are synthesized in Table 2. All operating conditions correspond to hydrogen hybridization rates higher than 65% in terms of power and equivalence ratio in the range of interest defined in Section 3.1. Two distinct regimes clearly appear, with a group of hole-initiated flashbacks for wall temperatures that do not exceed about 1000 K, and wall-initiated flashbacks that take place at higher wall temperatures, $T_w > 1050$ K. These results validate the importance of the crossover temperature, above which the autoignition delay was shown to drop drastically in Section 3.4. A criterion is now proposed to examine conditions leading to autoignition.

3.6. Transition criterion for autoignition

To confirm the possibility for autoignition to take place, the autoignition delay time τ_i must be compared to a residence time of fresh gases in the immediate vicinity of the wall. A residence time can be defined as $\tau_r = L_w/U_b$, L_w being the width of the weld considered as a characteristic length, and U_b the bulk velocity of the reactants flowing through a single hole at T_u.

The ratio τ_r/τ_i corresponds to a Damkohler number, as it compares a convective mass transport rate to a chemical time scale:

$$Da_i = \frac{\tau_r}{\tau_i} = \frac{L_w}{U_b}\frac{1}{\tau_i} \tag{3}$$

The autoignition Damkohler number Da_i is calculated for the operating conditions explored in Table 2 and results are plotted in Figure 14 as a function of the velocity ratio U_b/S_L determined for gases at $T_{u,f}$. The diagram highlights two different

regimes with Da_i values separated by one to two orders of magnitude between flashback initiated through a hole, regime FB-H, and flashback iniated agaisnt a hot wall, regime FB-AI. The possibility of autoignition is supported by the comparison between the flow time scale and chemical time scale, as the time spent by the reactants next to the hot wall appears long enough to overcome the delay needed by the combustible mixture to autoignite. Regime FB-H seems unlikely to be driven by autoignition, as the flow time scale remains small compared to chemical time scale

Table 2: Flashback regimes as a function of H_2-hybridization rate in power PH_2, total power P, equivalence ratio ϕ, wall temperature at flashback $T_{w,f}$, calculated unburnt gas temperature at flashback $T_{u,f}$, the velocity ratio U_b/S_L at $T_{u,f}$, the autoignition Damkohler number Da_i and location of flashback initiation.

PH_2 (%)	ϕ	Power (kW)	$T_{w,f}$ (K)	$T_{u,f}$ (K)	$(U_b/S_L)_{T_u}$	$Da_i = \frac{\tau_r}{\tau_i}$	Initiation location
100	0.6	3	953	705	0.64	0.13	Hole
100	0.61	3	940	696	0.63	0.03	Hole
88	0.67	3	953	705	0.61	0.14	Hole
85	0.70	3	950	703	0.59	0.11	Hole
85	0.72	3	937	694	0.57	0.03	Hole
72	0.71	3	1050	777	0.59	2.8	Wall
68	0.73	3	1055	781	0.59	3.0	Wall
67	0.75	3	1058	783	0.57	2.6	Wall
67	0.75	3.25	1053	779	0.62	2.3	Wall
67	0.75	3.5	1058	783	0.67	2.3	Wall
65	0.78	3	1067	790	0.55	2.8	Wall
65	0.78	3.5	1079	799	0.63	2.7	Wall
65	0.78	5	1081	800	0.89	1.9	Wall

in this case.

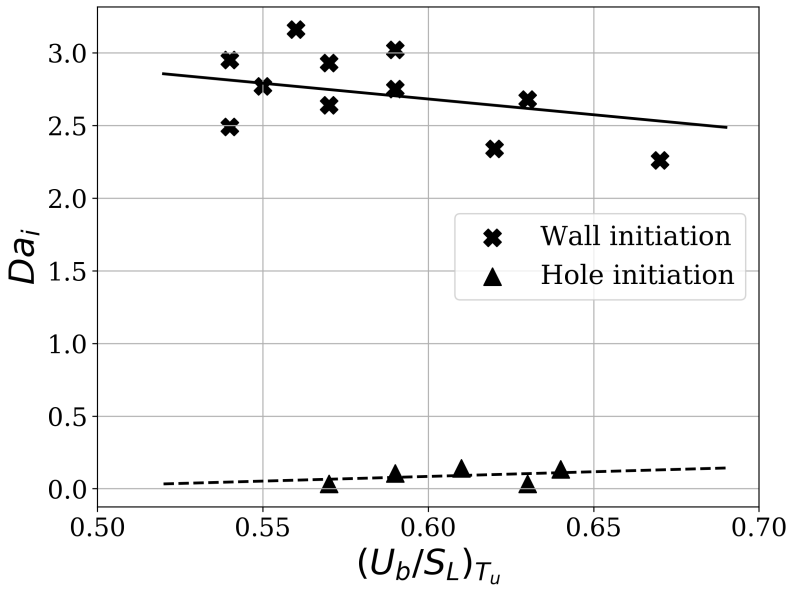

Figure 14: Comparison of autoignition Damkohler number $Da_i = \tau_r/\tau_i$ in regimes FB-H (triangle markers) and FB-AI (X markers).

Autoignition occurs mainly at the weld, but not systematically. Such events were also identified at other wall locations in some experiments. One example of initiation at the wall between two holes is presented in Figure 15. These events are yet marginally observed, because of the preferential spot that the weld represents.

Another important aspect to keep in mind is that the welding is carried out by laser fusion of the material, without addition of extra material, meaning that no specific surface reaction are expected to take place at the weld location with respect to the rest of the metallic wall. The mechanical and transport properties may have slightly changed for the welded section, but the observation of autoignition at other locations under the burner wall tends to confirm that the weld only provides a large unperforated hot surface, making it a preferential ignition location. Reducing or

removing the weld would most likely only shift the autoignition limit, due to a shorter residence time of the combustible mixture flowing along the wall.

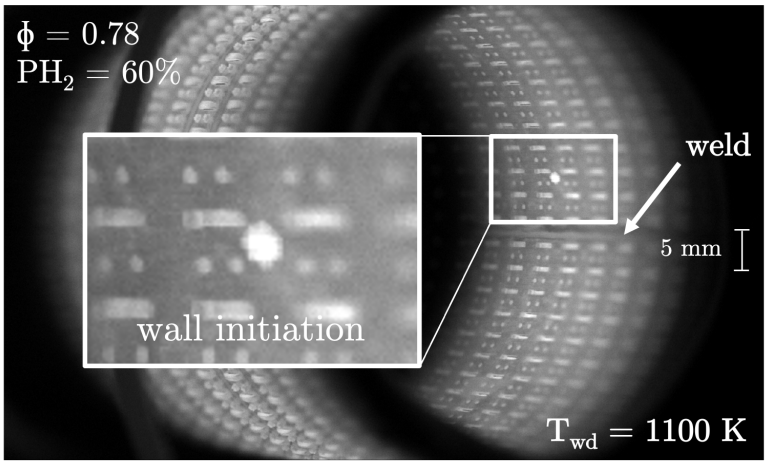

Figure 15: Example of initiation at the burner wall between two holes. $\phi = 0.78$, $PH_2 = 60\%$, $P = 3$ kW.

In Appendix B, an alternative technique is presented to identify unambiguously the flashback regime with the help of a photomultiplier. Flashback triggered by autoignition appears to initiate much faster than flashback resulting from upstream flame propagation through a hole. This translates to different signatures recorded by the photomultiplier for the FB-AI and FB-H regimes.

Figure 16 maps these different regimes in a stability diagram as a function of equivalence ratio ϕ and hydrogen hybridization rate PH_2, for a given thermal power $P = 3$ kW. Regime boundaries are delineated. Stable operation at the bottom left corner can only be sustained by lowering the equivalence ratio as the hydrogen hybridization rate is increased.

Instantaneous flashback right after ignition of the cold burner is observed at the top right corner for combustible with a high hydrogen content approaching stoichiometry.

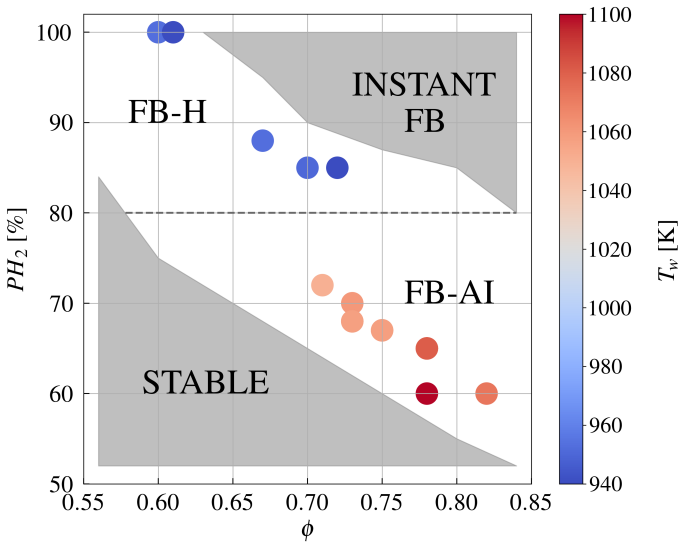

Figure 16: Burner stabilization map as a function of the hydrogen hybridization power rate and equivalence ratio. Studied operating points are colored by the temperature $T_{w,f}$ reached by the burner wall at flashback. $P = 3$ kW.

In between these two regimes, the inclined white band corresponds to flashback taking place during the thermal transient after ignition. In this case, flashback can be initiated by upstream flame propagation through a hole, the FB-H regime, occurring essentially for lean mixtures with a high hydrogen hybridization rate. But flashback can also be triggered by autoignition of the combustible mixture, inside the burner that flows against the hot metal, the FB-AI regime. It takes place at higher equivalence ratios but lower hydrogen hybridization rates. The limit between these flashback regimes mainly depend on the temperature of the metallic walls of the burner. If the hole size is further reduced while keeping a constant porosity, the flame would likely be unable to propagate upstream through a hole without being quenched. It such cases, autoignition could potentially become the only regime of flashback.

These experiments confirm the critical role of the burner wall thermal state in the occurrence of flashback events. The fundamental mechanisms that drive these processes were also elucidated. They lead to rethink the way premixed burners need to be adapted to fuel mixtures with increasing hydrogen contents.

4. Conclusion

Flashback in H_2-enriched premixed burners has been investigated, exploring the possibility of autoignition events as a function of equivalence ratio, H_2-hybridization rate and power. In these experiments, the adiabatic flame temperature was kept constant at a reference value corresponding to operation with natural gas. A specific experimental setup has been developed to provide a large optical access inside a generic domestic boiler burner. High-speed intensified imaging coupled to a photomultiplier has been used to explore flashback initiation and propagation inside the burner. It was found that the hottest spots of the burner wall constitute preferential initiation zones for flashback due to a higher preheat of the fresh reactants and a longer residence time.

Further experiments focusing on the flashback initiation region provided clear evidence for the existence of two regimes depending on the burner wall temperature. In the FB-H regime, FlashBack driven by Hydrodynamics, the initiation of flashback takes place inside a burner hole with a flame propagating upstream through the hole. This regime is observed for moderately hot burner walls, below 950 K. In the second FB-AI regime, FlashBack driven by AutoIgnition, spontaneous auto-ignition arises directly from the burner wall when the surface is hot enough, above 1000 K. Analysis of the initiation points distribution confirmed the highly repeatable nature of these different flashback regimes for a given thermal state of the burner and given combustible mixture composition.

An autoignition Damkohler number Da_i has been introduced, comparing a residence time of reactants flowing along the hot wall and the autoignition delay time. Comparison of Da_i for operation at constant $(U_b/S_L)_{T_u}$ revealed a gap larger than one order of magnitude between FB-H and FB-AI regimes. This low order model corroborates the existence of two mechanisms, the FB-H regime being initiated by a hydrodynamic imbalance leading to a flame moving upstream, and the FB-AI regime being driven by autoignition of the combustible mixture impinging the hot wall.
These findings may have important repercussions on the design of hydrogen-enriched premixed laminar burners. Due to the considerable wall temperature reached with hydrogen enriched mixtures, flashback can be driven by autoignition which shifts the expected flashback limit. Attention must therefore be paid to the control of the burner thermal state, in addition to the hydrodynamic equilibrium between the flow velocity and flame speed.

5. Acknowledgments

We acknowledge the support received from the SERMETA Research and Development Laboratory. We also acknowledge the funding received from the Association Nationale Recherche Technologie (ANRT) through the CIFRE grant n° 2021/1069. This project has received funding from the European Union's HORIZON 2020, European Research Council (ERC), Grant agreement 832248 SCIROCCO and under the Horizon 2020, COEC (Center of Excellence in Combustion) program, Grant Agreement 952181. We acknowledge the support of S. Cazin, G. Albert, S. Lun and L. Mouneix in the development of the experimental setup.

Appendix A. Impact of radiative heat transfer on the gas temperature measurements

The experimental procedure described in Section 2 of the manuscript to measure the temperature of the gas T_u does not consider the impact of the radiative heat transfer between the hot burner wall and the thermocouple bead. Hence, to prove the consistency of these measurements, additional experiments have been conducted to isolate the influence of the burner wall radiation on the experimental results.

The adopted procedure is the following: the burner is kept ignited until the wall temperature reaches 1000 K, which is representative of the cases investigated throughout the study. Then, the fuel is shut off. When the flame is quenched, the air is shut off as well. At this point, the thermocouple is placed next to the burner wall and the temperature is recorded. In this case, the only difference with respect to the original gas temperature measurements (see Section 2) consists in the absence of convection generated by the air stream. As a result, the temperature measurement depends only on natural convection and on the extent of the radiative heat transfer between the burner walls and the thermocouple bead which, in turn, can be estimated.

Results are presented in Figure 17. First, the increase of temperature recorded by the thermocouple remains below 30 K. This value is not only negligible when compared to the values of T_u measured in this study, but it is also overestimated with respect to the normal procedure. In fact, when air keeps flowing through the burner perforation, the temperature of the burner drops more rapidly and the effect of the wall radiation is quickly suppressed. This effect is also reported in Figure 17 that displays the evolution of the burner wall temperature with the air stream convection ($T_{w,cv}$) and without air stream (T_w).

These results show a negligible impact of radiative heat transfer on the gas temperature measured by the thermocouple and validate the experimental procedure adopted in Section 2.

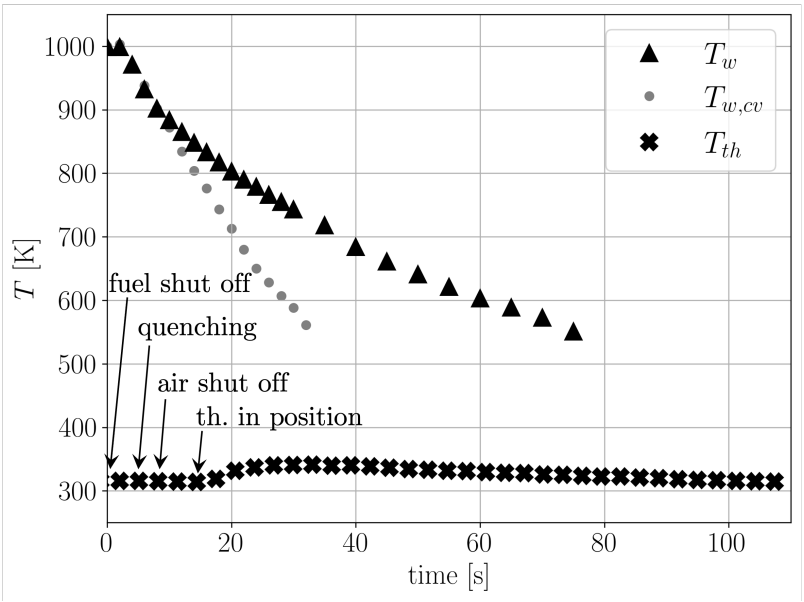

Figure 17: Impact of radiative heat transfer on the thermocouple measurement, $T_{w,0} = 1000$ K, $\phi = 0.65$, $PH_2 = 50\%$, $P = 3$ kW. Cross markers represent the temperature measured by the thermocouple, triangle markers correspond to the wall temperature measured by the pyrometer. The dotted line illustrates the wall temperature measured in the same situation without shutting off the air flowrate.

Appendix B. Alternative regimes discrimination

An alternative method is presented to infer the nature of the flashback regime based on records of the overall OH^* emission during transition to flashback with a photomultiplier placed in front of the optical access.

Because of the different initiation mechanisms between the two flashback regimes, a distinct signature in the initial dynamics of the PM signals is sought. Three signals

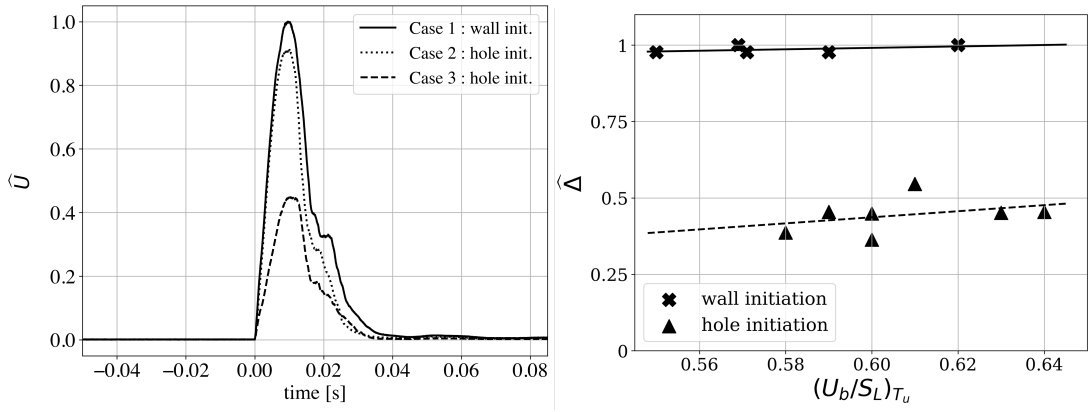

(a) scaled PM signal (b) scaled PM signal initial curvature

Figure 18: (a): comparison of scaled PM signals U during flashback for 3 flames at 3 kW: $PH_2 = 100\%$ and $\phi = 0.60$ (case 1), $PH_2 = 70\%$ and $\phi = 0.73$ (case 2) and $PH_2 = 85\%$ and $\phi = 0.70$ (case 3). (b): scaled PM signal initial curvature Δ for the operating conditions in Table 2 of the manuscript.

$\hat{U}(t) = OH^*(t)/OH^*_m$, where the OH* signal intensity is normalized by its maximum value OH$^*_m$, recorded during flashback are plotted in Figure 18a. Neither the height of the signal peak nor the slope of the PM response are specific to autoignition or flame moving upstream inside a hole. The signal recorded for case 2 associated to flashback initiation from a hole is closer to the signal recorded for case 3 corresponding to flashback initiated at the wall than signal 1 associated to another flashback initiated from a hole. This is consistent with the fact that, independently of the initiation mechanism, the light recorded after initiation corresponds to similar behaviors with a deflagration wave propagating inside the burner (see Figure 12 of the manuscript). These signals therefore mainly depend on flame speed, preheat gas temperature and wall temperature, independently of the mechanism at the origin of the flashback. However, the initiation is specific to each flashback mechanism. The curvature at

the very first instants of initiation t_f is a trace of the flame acceleration, which is expected to be higher in the case of autoignition compared to a flame front already established and propagating upstream through a hole. This is corroborated by some recent investigations with hydrogen enriched mixtures in canonical configurations [56, 57]. Auto-ignited combustible mixtures appear to be able to propagate against an inlet flow much faster than the flame speed of these mixtures. The signal initial curvature is deduced here from the PM intensity:

$$\Delta = \left.\frac{d^2U}{dt^2}\right|_{t=t_f} \tag{4}$$

The initial curvature normalized by its maximum value is plotted in Figure 18b for the operating conditions in Table 2 of the manuscript. In these experiments, attention was paid to keep the ratio $(U_b/S_L)_{T_u}$ roughly constant to limit the impact of kinematic imbalance between flow velocity and flame speed. The normalized value $\hat{\Delta}$ remains roughly constant for a given regime and its value doubles when switching from a hole initiation to an autoignition flashback regime. This additional test further confirms the duality observed with high-speed imaging and Da_i calculations, highlighting two distinct mechanisms of flashback featuring different origins and dynamics.

Appendix C. Supplementary material

Supplementary videos of flashback in the two regimes can be found in the online version.

References

[1] S. Griffiths, B. K. Sovacool, J. Kim, M. Bazilian, J. M. Uratani, Industrial decarbonization via hydrogen: A critical and systematic review of developments,

socio-technical systems and policy options, Energy Research & Social Science 80 (2021) Inpress. doi:10.1016/j.erss.2021.102208.

[2] T. Capurso, M. Stefanizzi, M. Torresi, S. Camporeale, Perspective of the role of hydrogen in the 21st century energy transition, Energy Conversion and Management 251 (2022) Inpress. doi:10.1016/j.enconman.2021.114898.

[3] H. Blanco, A. Faaij, A review at the role of storage in energy systems with a focus on power to gas and long-term storage, Renewable and Sustainable Energy Reviews 81 (2018) 1049–1086. doi:10.1016/j.rser.2017.07.062.

[4] G. Gahleitner, Hydrogen from renewable electricity: An international review of power-to-gas pilot plants for stationary applications, international Journal of hydrogen energy 38 (2013) 2039–2061. doi:10.1016/j.ijhydene.2012.12.010.

[5] A. Aniello, T. Poinsot, L. Selle, T. Schuller, Hydrogen substitution of natural-gas in premixed burners and implications for blow-off and flashback limits, International Journal of Hydrogen Energy 47 (2022) 33067–33081. doi:10.1016/j.ijhydene.2022.07.066.

[6] T. B. Kıymaz, E. Böncü, D. Güleryüz, M. Karaca, B. Yılmaz, C. Allouis, İskender Gökalp, Numerical investigations on flashback dynamics of premixed methane-hydrogen-air laminar flames, International Journal of Hydrogen Energy 47 (2022) 25022–25033. doi:10.1016/j.ijhydene.2022.05.230.

[7] Y. Zhao, V. McDonell, S. Samuelsen, Influence of hydrogen addition to pipeline natural gas on the combustion performance of a cooktop burner,

International Journal of Hydrogen Energy 44 (2019) 12239–12253. doi:10.1016/j.ijhydene.2019.03.100.

[8] S. Choudhury, V. G. McDonell, S. Samuelsen, Combustion performance of low-nox and conventional storage water heaters operated on hydrogen enriched natural gas, International Journal of Hydrogen Energy 45 (2020) 2405–2417.

[9] C. Meraner, T. Li, M. Ditaranto, T. Løvås, Cold flow characteristics of a novel bluff body hydrogen burner, International Journal of Hydrogen Energy 43 (2018) 7155–7168. doi:10.1016/j.ijhydene.2018.02.062.

[10] S.-S. Su, S.-J. Hwang, W.-H. Lai, On a porous medium combustor for hydrogen flame stabilization and operation, International journal of hydrogen energy 39 (2014) 21307–21316. doi:10.1016/j.ijhydene.2014.10.059.

[11] F. Halter, C. Chauveau, I. Gökalp, Characterization of the effects of hydrogen addition in premixed methane/air flames, International Journal of Hydrogen Energy 32 (2007) 2585–2592. doi:10.1016/j.ijhydene.2006.11.033.

[12] D. R. Jones, W. A. Al-Masry, C. W. Dunnill, Hydrogen-enriched natural gas as a domestic fuel: an analysis based on flash-back and blow-off limits for domestic natural gas appliances within the uk, Sustainable Energy & Fuels 2 (2018) 710–723. doi:10.1039/C7SE00598A.

[13] H. de Vries, A. V. Mokhov, H. B. Levinsky, The impact of natural gas/hydrogen mixtures on the performance of end-use equipment: Interchangeability analysis for domestic appliances, Applied energy 208 (2017) 1007–1019. doi:10.1016/j.apenergy.2017.09.049.

[14] H. de Vries, H. B. Levinsky, Flashback, burning velocities and hydrogen admixture: Domestic appliance approval, gas regulation and appliance development, Applied Energy 259 (2020) Inpress. doi:10.1016/j.apenergy.2019.114116.

[15] M. Fukuda, K. Korematsu, M. Sakamoto, On quenching distance of mixtures of methane and hydrogen with air., Bulletin of the JSME 24 (1981) 1192–1197. doi:10.1299/jsme1958.24.1192.

[16] A. C. Benim, B. Pfeiffelmann, Prediction of burning velocity and quenching distance of hydrogen flames, Vol. 128, EDP Sciences, 2019. doi:10.1051/e3sconf/201912801012.

[17] C. K. Law, Combustion physics, Cambridge university press, 2010.

[18] J. Jarosinski, The thickness of laminar flames, Combustion and Flame 56 (1984) 337–342. doi:10.1016/0010-2180(84)90067-1.

[19] H. M. Altay, K. S. Kedia, R. L. Speth, A. F. Ghoniem, Two-dimensional simulations of steady perforated-plate stabilized premixed flames, Combustion Theory and Modelling 14 (2010) 125–154. doi:10.1080/13647831003660859.

[20] T. García-Armingol, J. Ballester, Operational issues in premixed combustion of hydrogen-enriched and syngas fuels, International Journal of Hydrogen Energy 40 (2015) 1229–1243.

[21] C. Jiménez, D. Fernández-Galisteo, V. N. Kurdyumov, Dns study of the propagation and flashback conditions of lean hydrogen-air flames in narrow channels: symmetric and non-symmetric solutions, International Journal of

Hydrogen Energy 40 (2015) 12541–12549. doi:10.1016/j.ijhydene.2015.07.037.

[22] Y. Zhao, V. McDonell, S. Samuelsen, Experimental assessment of the combustion performance of an oven burner operated on pipeline natural gas mixed with hydrogen, International Journal of Hydrogen Energy 44 (2019) 26049–26062. doi:10.1016/j.ijhydene.2019.08.011.

[23] B. Lewis, G. V. Elbe, Stability and structure of burner flames, The Journal of Chemical Physics 11 (1943) 75–93. doi:10.1063/1.1723808.

[24] G. V. Elbe, M. Mentser, Further studies of the structure and stability of burner flames, The Journal of Chemical Physics 13 (1945) 89–100. doi:10.1063/1.1724004.

[25] B. A. A. Putnam, R. A. Jensen, Application of dimensionless numbers to flashback and other combustion phenomena, Symposium on Combustion and Flame, and Explosion Phenomena 3 (1976) 89–98. doi:10.1016/S1062-2896(49)80011-0.

[26] A. Kalantari, V. McDonell, Boundary layer flashback of non-swirling premixed flames: Mechanisms, fundamental research, and recent advances, Progress in Energy and Combustion Science 61 (2017) 249–292. doi:10.1016/j.pecs.2017.03.001.

[27] J. Grumer, M. E. Harris, Temperature dependence of stability limits of burner flames, Industrial and Engineering Chemistry 46 (1954) 2424–2430. doi:10.1021/ie50539a057.

[28] G. L. Dugger, Flame stability of preheated propane-air mixtures, Industrial and Engineering Chemistry 47 (1955) 109–114. doi:10.1021/ie50541a038.

[29] C. Law, Dynamics of stretched flames, in: Symposium (international) on combustion, Vol. 22, Elsevier, 1989, pp. 1381–1402. doi:10.1016/S0082-0784(89)80149-3.

[30] F. A. Williams, Combustion theory, CRC Press, 2018. doi:10.1201/9780429494055.

[31] M. Mizomoto, Y. Asaka, S. Ikai, C. Law, Effects of preferential diffusion on the burning intensity of curved flames, in: Symposium (International) on Combustion, Vol. 20, Elsevier, 1985, pp. 1933–1939. doi:10.1016/S0082-0784(85)80692-5.

[32] F. H. Vance, P. de Goey, J. A. van Oijen, The effect of thermal diffusion on stabilization of premixed flames, Combustion and Flame 216 (2020) 45–57. doi:10.1016/j.combustflame.2020.02.006.

[33] F. Dabireau, B. Cuenot, O. Vermorel, T. Poinsot, Interaction of flames of h2 + o2 with inert walls, Combustion and Flame 135 (2003) 123–133. doi:10.1016/S0010-2180(03)00154-8.

[34] K. S. Kedia, A. F. Ghoniem, The blow-off mechanism of a bluff-body stabilized laminar premixed flame, Combustion and Flame 162 (2015) 1304–1315. doi:10.1016/j.combustflame.2014.10.017.

[35] C. Jainski, M. Rißmann, B. Böhm, J. Janicka, A. Dreizler, Sidewall quenching of atmospheric laminar premixed flames studied by laser-based diagnostics,

Combustion and Flame 183 (2017) 271–282. doi:10.1016/j.combustflame.2017.05.020.

[36] H. Kosaka, F. Zentgraf, A. Scholtissek, C. Hasse, A. Dreizler, Effect of flame-wall interaction on local heat release of methane and dme combustion in a side-wall quenching geometry, Flow, Turbulence and Combustion 104 (2020) 1029–1046. doi:10.1007/s10494-019-00090-4.

[37] C. Sun, C.-J. Sung, L. He, C.-K. Law, Dynamics of weakly stretched flames: quantitative description and extraction of global flame parameters, Combustion and flame 118 (1999) 108–128. doi:10.1016/S0010-2180(98)00137-0.

[38] L. Berger, A. Attili, H. Pitsch, Intrinsic instabilities in premixed hydrogen flames: Parametric variation of pressure, equivalence ratio, and temperature. part 1 - dispersion relations in the linear regime, Combustion and Flame 240 (2022) Inpress. doi:10.1016/j.combustflame.2021.111935.

[39] L. Berger, A. Attili, H. Pitsch, Intrinsic instabilities in premixed hydrogen flames: parametric variation of pressure, equivalence ratio, and temperature. part 2 – non-linear regime and flame speed enhancement, Combustion and Flame 240 (2022) Inpress. doi:10.1016/j.combustflame.2021.111936.

[40] F. Vance, L. de Goey, J. van Oijen, Development of a flashback correlation for burner-stabilized hydrogen-air premixed flames, Combustion and Flame 243 (2022) Inpress. doi:10.1016/j.combustflame.2022.112045.

[41] K. Aung, M. Hassan, G. Faeth, Effects of pressure and nitrogen dilution on flame/stretch interactions of laminar premixed h2/o2/n2 flames, Combustion and flame 112 (1998) 1–15. doi:10.1016/S0010-2180(97)81753-1.

[42] V. Hoferichter, C. Hirsch, T. Sattelmayer, Prediction of confined flame flashback limits using boundary layer separation theory, Journal of Engineering for Gas Turbines and Power 139 (2017) Inpress. doi:10.1115/1.4034237.

[43] V. Hoferichter, C. Hirsch, T. Sattelmayer, Prediction of boundary layer flashback limits of laminar premixed jet flames, in: Turbo Expo: Power for Land, Sea, and Air, Vol. 51050, American Society of Mechanical Engineers, 2018. doi:10.1115/GT2018-75546.

[44] A. M. Gamal, A. H. Ibrahim, E.-M. M. Ali, F. M. Elmahallawy, A. Abdelhafez, M. A. Nemitallah, S. S. Rashwan, M. A. Habib, Structure and lean extinction of premixed flames stabilized on conductive perforated plates, Energy & Fuels 31 (2017) 1980–1992. doi:10.1021/acs.energyfuels.6b02874.

[45] R. Lamioni, C. Bronzoni, M. Folli, L. Tognotti, C. Galletti, Feeding h2-admixtures to domestic condensing boilers: Numerical simulations of combustion and pollutant formation in multi-hole burners, Applied Energy 309 (2022) Inpress. doi:10.1016/j.apenergy.2021.118379.

[46] M. S. Boulahlib, F. Medaerts, M. A. Boukhalfa, Experimental study of a domestic boiler using hydrogen methane blend and fuel-rich staged combustion, International Journal of Hydrogen Energy 46 (2021) 37628–37640. doi:10.1016/j.ijhydene.2021.01.103.

[47] Y. Jung, M. J. Lee, N. I. Kim, Direct prediction of laminar burning velocity and quenching distance of hydrogen-air flames using an annular stepwise diverging tube (asdt), Combustion and Flame 164 (2016) 397–399. doi:10.1016/j.combustflame.2015.12.005.

[48] R. K. Cheng, A. K. Oppenheim, Autoignition in methanehydrogen mixtures, Combustion and Flame 58 (1984) 125–139. doi:10.1016/0010-2180(84)90088-9.

[49] N. Donohoe, A. Heufer, W. K. Metcalfe, H. J. Curran, M. L. Davis, O. Mathieu, D. Plichta, A. Morones, E. L. Petersen, F. Güthe, Ignition delay times, laminar flame speeds, and mechanism validation for natural gas/hydrogen blends at elevated pressures, Combustion and Flame 161 (2014) 1432–1443. doi:10.1016/j.combustflame.2013.12.005.

[50] C. Trevino, F. Méndez, Asymptotic analysis of the ignition of hydrogen by a hot plate in a boundary layer flow, Combustion Science and Technology 78 (1991) 197–216. doi:10.1080/00102209108951749.

[51] G. D. Álamo, F. A. Williams, A. L. Sánchez, Hydrogen-oxygen induction times above crossover temperatures, Combustion Science and Technology 176 (2004) 1599–1626. doi:10.1080/00102200490487175.

[52] A. L. Sánchez, F. A. Williams, Recent advances in understanding of flammability characteristics of hydrogen, Progress in Energy and Combustion Science 41 (2014) 1–55. doi:10.1016/j.pecs.2013.10.002.

[53] R. W. Schefer, W. D. Kulatilaka, B. D. Patterson, T. B. Settersten, Visible emission of hydrogen flames, Combustion and Flame 156 (2009) 1234–1241. doi:10.1016/j.combustflame.2009.01.011.

[54] Y. Ding, D. Durox, N. Darabiha, T. Schuller, Chemiluminescence of burner-stabilized premixed laminar flames, Combustion Science and Technology 191 (2019) 18–42. doi:10.1080/00102202.2018.1558391.

[55] P. Boivin, Reduced-kinetic mechanisms for hydrogen and syngas combustion including autoignition (2011). doi:10016/13988.

[56] C. Xu, J.-W. Park, C. S. Yoo, J. H. Chen, T. Lu, Identification of premixed flame propagation modes using chemical explosive mode analysis, Proceedings of the combustion Institute 37 (2019) 2407–2415. doi:10.1016/j.proci.2018.07.069.

[57] A. Gruber, M. R. Bothien, A. Ciani, K. Aditya, J. H. Chen, F. A. Williams, Direct numerical simulation of hydrogen combustion at auto-ignitive conditions: Ignition, stability and turbulent reaction-front velocity, Combustion and Flame 229 (2021) Inpress. doi:10.1016/j.combustflame.2021.02.031.